Scripta Materialia 238 (2024) 115768

Contents lists available at ScienceDirect

Scripta Materialia

journal homepage: www.journals.elsevier.com/scripta-materialia

Identification, classification and characterisation of hydrides in Zr alloys

Mia Maric [a,*], Rhys Thomas [a], Alec Davis [a], David Lunt [a], Jack Donoghue [a], Ali Gholinia [a], Marc De Graef [b], Tamas Ungar [a], Pierre Barberis [c], Florent Bourlier [d], Philipp Frankel [a], Pratheek Shanthraj [a,e], Michael Preuss [a,f]

[a] Department of Materials, The University of Manchester, Manchester M13 9PL, UK
[b] Department of Materials Science and Engineering Carnegie Mellon University, Pittsburgh, PA, USA
[c] Framatome, CRC, Avenue Paul Girod, CS 90100, 73403 Ugine Cedex, France
[d] Framatome, 2 rue Professeur Jean BERNARD, 69007 Lyon, France
[e] United Kingdom Atomic Energy Authority, Culham, Abingdon, UK
[f] Department of Materials Science & engineering, Monash University, Clayton, Vic-3800, Australia

ARTICLE INFO

Keywords:
Dictionary Indexing
Zirconium Hydrides
Electron backscatter diffraction (EBSD)
Orientation relationship
Electron backscattering patterns (EBSP)

ABSTRACT

Hydride precipitation in zirconium alloys leads to embrittlement, making it essential to understand their prevalence and stability in the microstructure. Dictionary indexing of Kikuchi patterns, along with orientation relationship analysis and x-ray diffraction, confirmed the presence of both delta and gamma hydride phases in Zircaloy-4. Both phases were found to be stable in recrystallised zirconium, with the gamma phase exhibiting a distinct orientation relationship with the matrix. Delta hydride morphology and orientation were influenced by local stresses, resulting in a change in orientation during precipitation. By analysing the orientation relationships, the evolution of hydride phases could be visualised, providing insights into the room temperature stability of both delta and gamma hydrides.

Hydrogen precipitation is an embrittlement mechanism that can result in the premature failure of zirconium (Zr) alloys. Four hydride phases are commonly reported to precipitate in Zr: γ-ZrH, δ-$ZrH_{1.63}$, ς-Zr_2H and ε-ZrH_2 respectively [1–5]. Of these, the δ and γ phase have received the most attention owing to their stability under nuclear reactor conditions [6]. One of the most contentious topics within this field is the stability of the γ phase at room temperature. Recent studies suggest that alloy purity influences the prevalence of γ, whereby it was shown to be stable in high purity Zr [7–19]. Here, microstructural analysis highlighted that the hydride microstructure consists of a δ core surrounded by a γ fringe. On the other hand, the prevalence of γ at room temperature for alloyed Zr is scarce. It is typically only identified in significant quantities after quenching, suggesting that it is metastable [8,10,20–22]. Presently, factors promoting or inhibiting the formation of the γ phase are not well understood and are of constant debate.

Typically, transmission electron microscopy (TEM) and synchrotron X-ray diffraction (S-XRD) are utilised to characterise hydrides, but their associated errors and uncertainties may contribute to the lack of understanding of the γ phase stability [23]. For example, the techniques used to prepare hydrided Zr for TEM analysis can induce hydride defects that are indistinguishable from the original hydrides, making subsequent analysis on the microstructure unreliable [22]. Using S-XRD to identify γ can be challenging due to the very low volume fraction of hydrides, relatively weak scattering properties of hydrides and overlapping diffraction peaks [24].

To supplement these techniques, we developed a novel, reproducible experimental protocol employing electron backscatter diffraction (EBSD) in conjunction with dictionary indexing (DI) and orientation relationship (OR) analysis to identify and characterise Zr-hydrides. The combination of these two techniques enables visualisation of evolution of the hydride phase such that the stability of both γ and δ can be inferred.

In this study, recrystallised Zircaloy-4 cladding tubes were gas-charged to a hydrogen content of 360 wt. ppm and furnaced cooled at a rate of 1 °C/min. The gas hydriding was conducted at 400°C. More information on the samples' thermal, stress and hydriding history is detailed elsewhere [25]. The EBSD maps presented in this study focused on a single magnified hydride stringer that is separated by hydride free regions. For more information on this see [25]. The radial/transverse face of samples were mechanically polished and analysed on an FEI

* Corresponding author.
E-mail address: mia.maric@manchester.ac.uk (M. Maric).

https://doi.org/10.1016/j.scriptamat.2023.115768
Received 18 July 2023; Received in revised form 1 September 2023; Accepted 12 September 2023
Available online 21 September 2023
1359-6462/© 2023 The Authors. Published by Elsevier Ltd on behalf of Acta Materialia Inc. This is an open access article under the CC BY license (http://creativecommons.org/licenses/by/4.0/).

Magellan using a NordlysNano EBSD detector with AZTEC® 4.3. A beam current of 1.6 nA, accelerating voltage of 20 keV and step size of 0.1 μm at an acquisition speed of 1.87 Hz was utilised for EBSD collection. All Kikuchi patterns have a resolution of 672 × 512 pixels and were stored for further post processing. The EBSD maps were generated and processed in AZtecCrystal.

Both Hough and Dictionary based indexing (DI) methods were utilised and compared. Hough Indexing (HI) initially identifies the locations of Kikuchi bands within a pattern. The angle between the bands is compared with known values for a particular crystal system to identify phases and orientations within the material [26]. In contrast, DI employs a physics based forward model to generate all possible patterns representing a particular crystal structure. These are compared to each experimentally obtained Kikuchi pattern to obtain a dot product [27–29]. The simulated orientation with the highest dot product is assigned to that point. The software used to perform DI was EMsoft 5.0 [30].

To obtain accurate information on the phases and orientations from DI, the Efit package in EMsoft was employed [30]. Here, a Zr reference pattern from the studied dataset with a high band to background contrast was refined. The pattern centre, scintillator distance and detector pixel size were refined from the initial AZtec derived values. Prior to indexing, the patterns were binned four times to reduce the pattern noise, ensuring that pattern noise was not affecting the indexing and effective indexing of the hydride patterns could be obtained. The crystal structures were assigned as face centre cubic (FCC) with space group $Fm\bar{3}m$ lattice parameter a_o= 4.778 Å for the δ phase [31–42] and face centred tetragonal structure with space group $P4_2/n$ and lattice parameters a_o= 4.586 Å and c_o = 4.948 Å for the γ phase [10,11,19,23, 37–40]. The final stage in DI analysis was to perform orientation refinement using EMFitOrientation [30]. DefDAP [41] was utilised to compute differences in orientation between DI and HI.

HI was first optimised to improve the extent of indexing whilst retaining accuracy. This is particularly important for large-scale EBSD maps, where storing patterns and DI searches is not practical. The effect of the maximum number of Kikuchi bands used and the Hough Resolution (HR), which sets the Hough space resolution for band detection, were investigated. Owing to the high similarity and low signal-to-noise of the γ and δ hydride patterns, only the δ phase was indexed in AZtec to avoid additional mis-indexing between the two phases during collection.

The influence of the maximum number of bands (MBN) is shown in Fig. 1a-c). Here, AD, RD and TD are the axial, tangential and radial direction respectively. In these three cases, the HR and number of reflectors for the hydride phase were kept constant at 60 and 44 respectively. The reflectors being the 44 strongest calculated bands for each crystal system that the Hough transformed pattern is compared against for indexing. The variation in indexing at the different band levels is shown in Fig. 1d and e. Here, the overall extent of hydride and total indexing as a function of the MBN at a HR of 60 and 80 is plotted in blue and red respectively. A peak in hydride indexing at a MBN of 11 and HR of 60 is apparent and will be discussed in detail in this study. The extent of indexing at MBNs either side of this peak at both HRs is discussed in S1.

To understand the peak in indexing at an MBN of 11, it is important to note that when the MBN is 7-11, a minimum of 6 bands must fit for indexing (see S1 for more details). Thus, when a minimum of 6 bands need to fit, then the greatest difference between the maximum and minimum band number values occurs at an MBN of 11. The greater difference in band number allows for a larger number of bands to be indexed by the software. This increased tolerance enables the weaker hydride bands to be indexed with greater confidence reducing the influence of pattern overlap on hydride indexing. The accuracy of the indexing is highlighted by comparing the indexed points to the DI map in Fig. 1 f. Further, reducing the HR at an MBN value of 11 improves

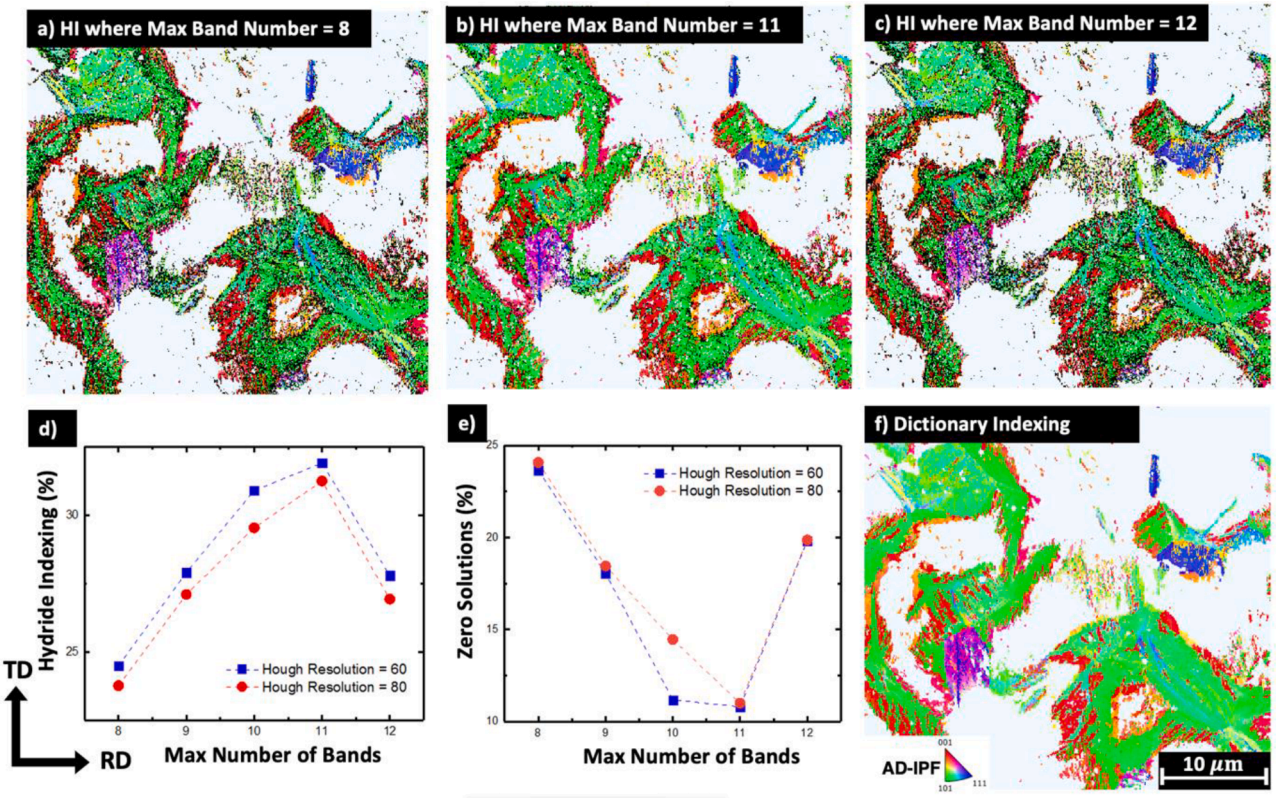

Fig. 1. The white, AD-IPF colours and black regions are the Zr, Hydride and un-indexed hydride pixels, respectively. a-c) are Hough indexed AD-IPF maps at MBNs of 8,11 and 12 and HR=60. d-e) Plot the percentage of hydride and un-indexed points as the MBN and HR is altered. f) AD-IPF map after DI. Note that the EBSD dataset above used has been initially presented in Maric et al. [25].

indexing by 3% as there is greater tolerance for band position, enabling a greater proportion of the deformed hydride bands to be detected. The optimisation of MBN and HR improved hydride indexing by up to 10%, highlighting the importance of adjusting HI parameters when differentiating between multi-phase materials with varying pattern qualities.

However, differentiating between the γ and δ hydride phase, which are crystallographically similar and highly deformed, using HI was not feasible. The effectiveness of HI strongly depends on the pattern quality so weak patterns with low band to background contrast will have poor indexing and reduced accuracy [42]. When DI was employed (Fig. 2a), γ hydride has been effectively indexed on the fringes of the δ/α-Zr phase boundary as observed in previous studies [7,9,10,19].

XRD was utilised to verify the DI results and identify the γ-phase (experimental details in S2). The low γ volume fraction and overlapping reflections from other phases meant only a small $\{111\}_\gamma$ peak (2.7 Å) shown by the blue circle could be conclusively observed (Fig. 2b), however this correlates well to the small extent of γ-hydride identified by EBSD.

Fig. 2c-e plot the dot product, γ-H and δ-H IPF maps, respectively. A value closer to one indicates a greater correlation between the simulated and experimental patterns. The dot product is substantially lower for the hydride phase than the α-Zr. This could be due to the greater misorientation and strain within and around the hydride grains resulting in a lack of discrete patterns when compared to recrystallised α-Zr. See S2 for analysis on the difference in deformation between the hydride and matrix phase.

From the IPF maps in Fig. 2d, e and Fig. 1f, a fringe can be identified on δ and α-Zr phase boundary. The fringe has a 45° shift in orientation from <101> to the <001> fibre direction when compared to the bulk hydrides it encases. When comparing the phase and IPF map, DI identifies both δ and γ hydride within the fringe region. Here, areas of high and low dot product exist. As shown by the red circles in Fig. 2c, high dot product regions on the exterior of the fringe typically index as γ, whilst the neighbouring fringe regions have a lower dot product and index as δ.

Both the δ and γ phases present within the fringe are oriented in the <001>//AD in contrast to the bulk δ oriented in the <111>//AD direction. The origin of the shift in δ phase orientation has been related back to the increased thermal expansion and volumetric mismatch that occurs during hydride precipitation [6,43,44]. Kerr et al. [45] also observed δ hydrides oriented in the two aforementioned directions where the difference was attributed to high transformation stresses imparted on the microstructure during cooling. The weaker patterns coupled with the change in orientation of the δ phase at the fringe alludes to the formation of a more deformed δ phase that adopts a different orientation to better accommodate the increased stress. However, due to the poor contrast in the Kikuchi patterns stemming from the high level of deformation and potential pattern overlap, TEM studies of this region are required to further confirm the presence of γ and δ phases.

Furthermore, a distinguishing feature between hydrides of different phases and orientations is the ORs that they have with the matrix material. It is important to note that EBSD rather than TEM is readily employed for hydride OR characterisation [45–47]. This is because, unlike TEM, bulk ORs at lower magnifications can be observed in addition to having simpler sample preparation techniques [47]. The most commonly observed OR between the δ phase and Zr matrix is $\{0001\}_\alpha||\{111\}_\delta$ and $\langle 11\bar{2}0\rangle_\alpha||\langle 110\rangle_\delta$ [21,47,48]. Whilst the minor $\{0001\}_\alpha||\{001\}_\delta$ and $\langle 11\bar{2}0\rangle_\alpha||\langle 1\bar{1}0\rangle_\delta$ OR have also been identified in highly stressed hydride regions [45]. In this study we will refer to the respective δ-hydride ORs as δ-Major and δ-Minor. Less research into the ORs between the γ phase and Zr matrix is available, with belief that the γ phase was meta-stable limiting analysis at room temperature. However, with an increased number of studies reporting its stability, the following OR has been proposed: $\{0001\}_\alpha||\{001\}_\gamma$ and $\langle 11\bar{2}0\rangle_\alpha||\langle 1\bar{1}0\rangle_\gamma$ [49,50].

OR analysis was performed using the AZtecCrystal OR analysis tool inspired by Une et al. [47]. This technique was expanded allowing ORs across the whole micrograph to be visualised such that inferences about the order of hydride precipitation could be made. Fig. 3a plots the OR boundaries for γ, δ-Major and δ-Minor phases. The ORs plotted have a ± 10 ° tolerance to account for the high strain and hence potential OR mismatch that occurs during hydride precipitation. Both γ and δ

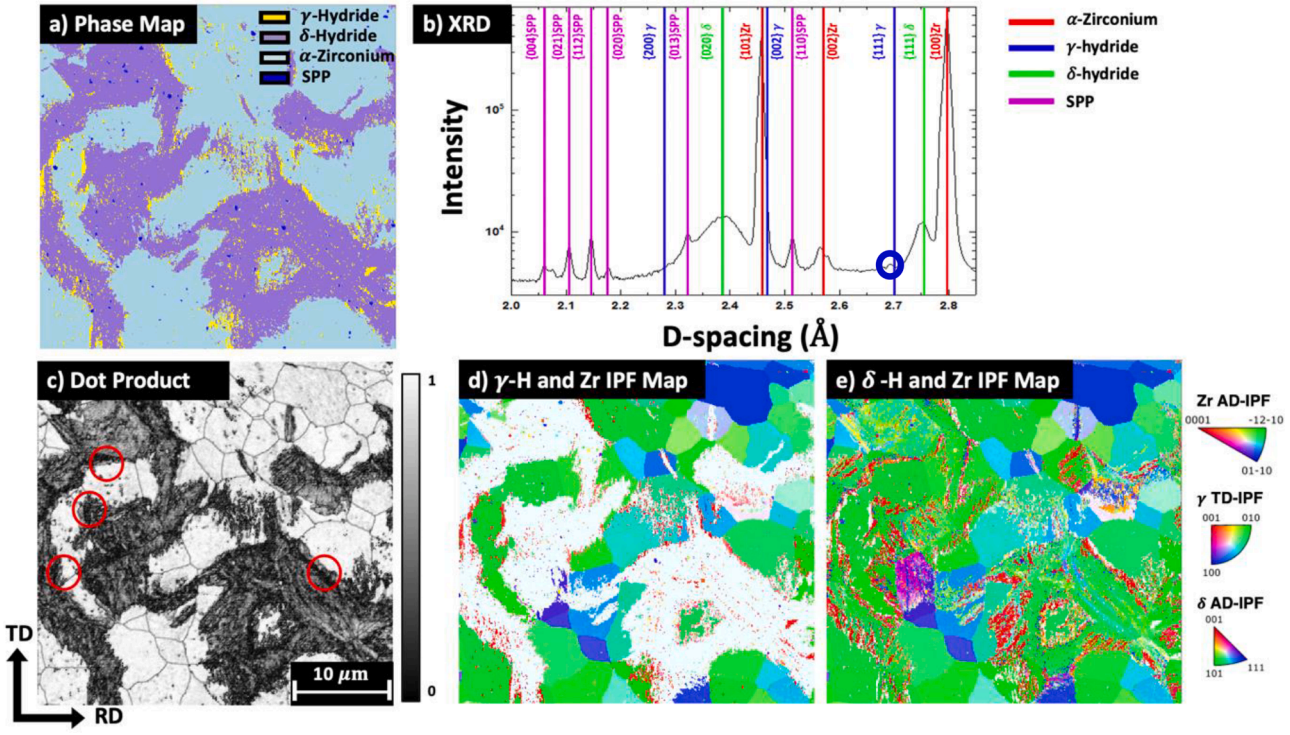

Fig. 2. a) is the phase map for α-Zr, δ-Hydride, γ-Hydride, and Secondary Phase Particles (SPP's), b) XRD phase identification c) The dot product map d,e) are IPF maps for the γ-H and δ-H phases.

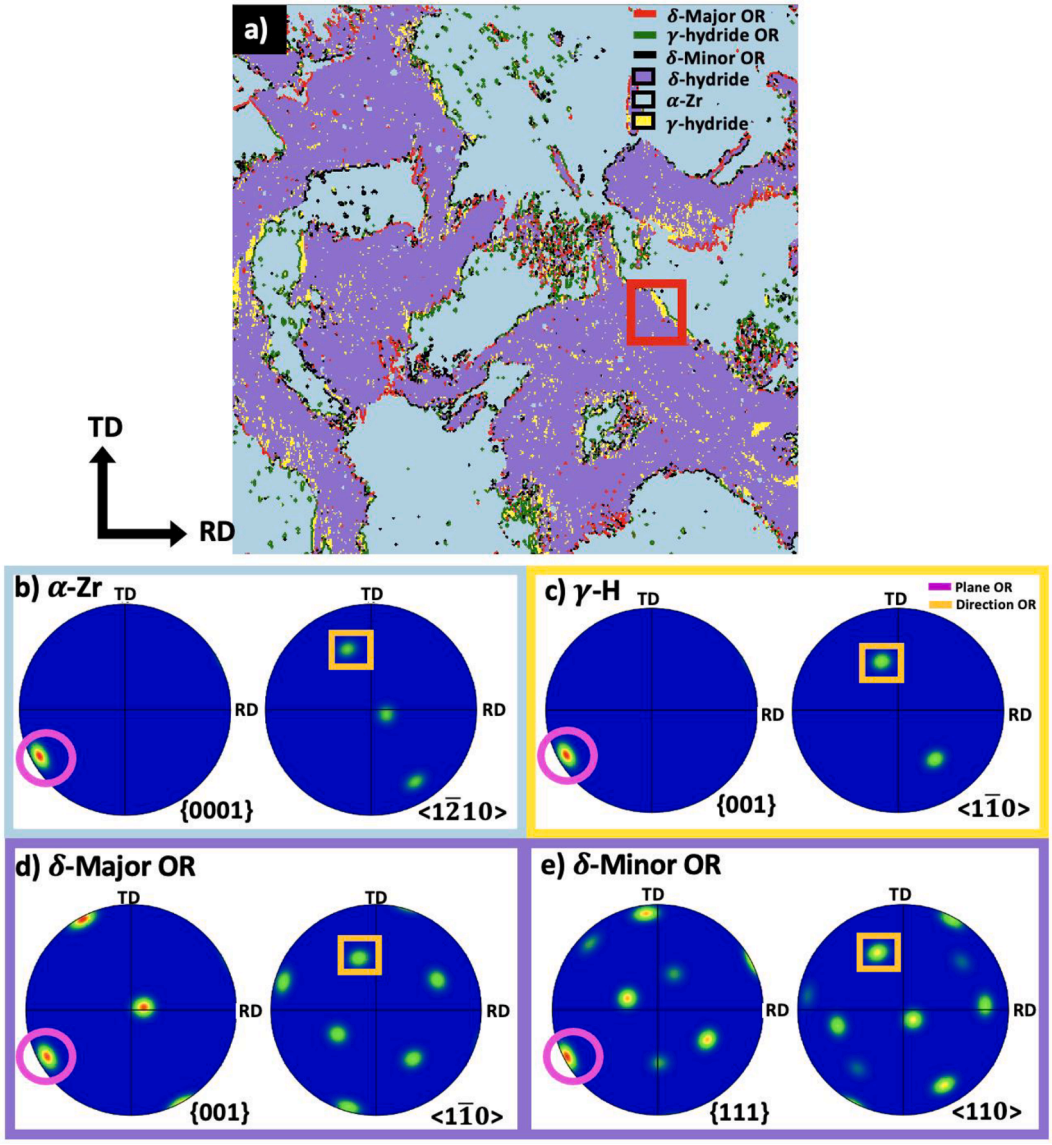

Fig. 3. a) Phase map where the green, red and black boundaries shown are phase boundaries that adhere ($\pm 10^{o}$) to the γ-Zr, δ-Minor and δ-Major ORs, respectively. The red rectangle is the region where localised OR analysis was conducted. b-e) are pole figures for the Zr, γ-hydride, δ-Minor and δ-Major phases within the red rectangle, where the pink circles and orange rectangles display the matching points within the respective pole figures for each phase. If the locations of the pink and orange points are identical between the different phases, then an OR exists between them.

hydrides located on the fringe adhere to γ and δ-Minor OR, respectively, whilst the bulk δ phase follows the δ-Major OR.

The fraction of boundaries adhering to each OR was investigated (Table 1), representing a dataset of ~100 Zr grains and ~10 hydride clusters. The greatest percentage of hydride-matrix boundaries comes from γ-Zr OR (38%), followed by the δ-Minor OR (36%). It is evident that the conventional $\{0001\}_{\alpha}||\{111\}_{\delta-Major}$ and $\langle 11\bar{2}0\rangle_{\alpha}||\langle 110\rangle_{\delta-Major}$ OR still populates around 26% of the hydride phase boundaries. To understand the origin and distribution of the δ-Major OR, analysis of the Zr grains where this OR is present was conducted. As highlighted in Figs. 2d and 3a, the Zr grains where the δ-Major OR is largely prevalent are mostly orientated close to the $\langle 10\bar{1}0\rangle$ direction. It could be that some grain orientations stabilise the δ hydride formation and inhibit γ formation more than others due to variations in their local stress states [24]. The change in stress conditions of these grains could also mean that less deformation is imparted onto the hydride during precipitation such that the δ phase precipitation adhering to the δ-Minor OR does not occur as readily. The mechanisms of this will be explored in a future study exploring correlations between grain orientations and hydride phase stability.

Table 1
Fraction of hydride phase boundaries that adhere to the γ, δ-Minor and δ-Major orientation relationship respectively.

Orientation Relationship (OR)	Length of hydride-matrix phase boundary that satisfies OR (μm)	Percentage of total hydride-matrix phase boundary that satisfies OR (%)
$\{0001\}_{\alpha}\langle 11\bar{2}0\rangle_{\alpha}\|\|$ $\{001\}_{\gamma} < 1\bar{1}0 >_{\gamma}$	488	38
$\{0001\}_{\alpha}\langle 11\bar{2}0\rangle_{\alpha}\|\|$ $\{001\}_{\delta-Minor} < 110 >_{\delta-Minor}$	459	36
$\{0001\}_{\alpha}\langle 11\bar{2}0\rangle_{\alpha}\|\|$ $\{111\}_{\delta-Major} < 110 >_{\delta-Major}$	343	26

A localised OR study was conducted on the region outlined by the red rectangle in Fig. 3a. Here, the TD/RD pole figures for the Zr, γ, δ-Minor

and δ-Major ORs are shown in Fig. 3b-e confirming the aforementioned ORs locally.

A δ-Major OR between the bulk δ phase and α-Zr exists even though there is no phase boundary between the two phases (Fig. 3b,e). This suggests that δ-Major is a high temperature stable phase that forms initially upon cooling. A schematic of the hydride precipitation sequence upon cooling based on the observed ORs is shown in Fig. 4. Initially, the δ phase precipitates at the grain boundaries of α-Zr grains resulting in the distinct δ-Major OR. As cooling proceeds, precipitation of δ hydride oriented in the <001> direction is promoted to accommodate the increased stress at the Zr-hydride phase boundary. The change in local stress conditions could cause the precipitating hydride to change orientation, forming a new OR with the Zr as shown by the blue rectangle in Fig. 4c. The extent of stress required for this change has not been investigated in this study but should be a focus of future studies.

After this at the final stages of cooling, γ forms at the edges of the phase boundary between the δ and α-Zr obeying the OR in the orange rectangle in Fig. 4d. By analysing the orientation distribution of these phases, the order of their formation, and hence stability upon cooling, can be better understood. Additionally, sharp transitions between the hydride phase boundaries are observed suggesting that the precipitation of γ and δ of different orientations occurs to accommodate for the altered stress and thermal states of the microstructure during cooling rather than being formed by slow diffusion related processes.

The formation of the γ phase at the end of cooling supports previous reports of its room temperature stability [7,9,10,19]. Further studies with increased ageing at room temperature are required to confirm this trend and better understand γ phase transformation kinetics.

This study details techniques developed to optimise and improve the indexing of multi-phase materials whilst retaining accuracy when utilising EBSD. We highlight the importance of optimising the HI parameters if the indexing efficiency for a particular material is to be maximised. By altering the MBN and HR for the Zr hydrides, we were able to improve the indexing by up to 10%. Moreover, when the pattern quality is poor and the crystal structures of the present phases are very similar, we highlight that DI can be employed to differentiate and characterise the phases. DI analysis highlighted the prevalence of three hydride variants within the microstructure, γ, <001> δ and <111> δ hydrides. The proportions and relative distributions of each phase could be visualised and mechanisms for their formation are proposed. Finally, OR analysis combined with phase identification has, for the first-time, enabled bulk characterisations of the evolution of the hydride phase upon cooling using EBSD. The location of hydrides adhering to different ORs has been correlated to their sequence of precipitation within the matrix, indicating that the γ hydride is the last to form at the Zr-Hydride phase boundary upon cooling; providing evidence that it is stable at room temperature in Zr alloys with reduced strength. The present study conducted both phase identification and OR analysis on the microstructure at the conclusion of precipitation. If the hypotheses proposed in this study are to be further validated, TEM as well as in-situ experiments observing hydride evolution during precipitation should be conducted and further developed.

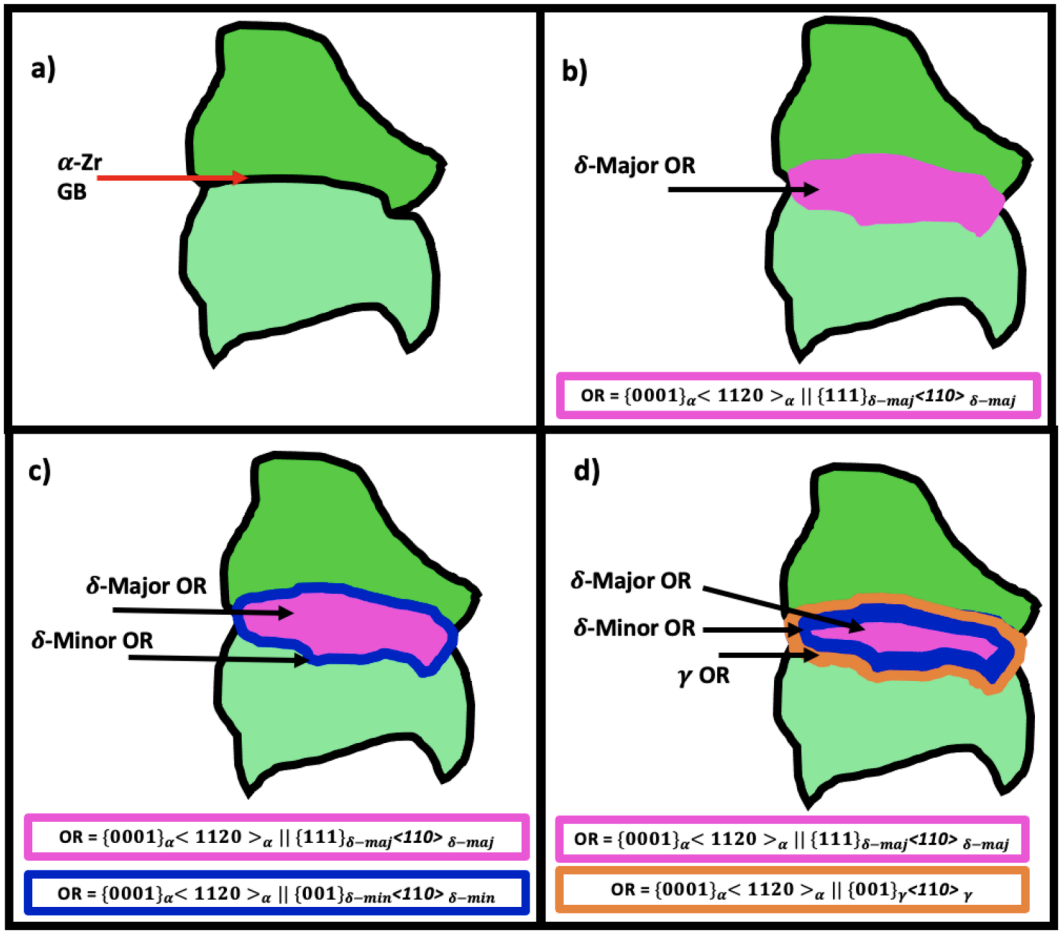

Fig. 4. Schematic of the proposed precipitation and evolution of δ and γ hydride upon cooling. Initially, a) there are two neighbouring Zr grains and then b) the δ phase forms adhering to the OR depicted by the pink rectangle. With further cooling, δ forms as a mechanism of stress accommodation adhering to the OR in the blue box in c). Additional cooling results in the formation of the γ phase at the γ– α Zr phase boundary following the OR shown in the orange rectangle in d). Here, a new technique for the characterisation of the evolution of the different hydride phases has been developed such that their order of formation can be determined.

Author Contributions

M.M, P.S, P.F, and M.P developed the project idea and scope and provided continuous feedback and support for the entire project. M.M and A.D conducted EBSD analysis with the guidance of J.D, D.L and A.G. M.M, R.T and M.DG conducted dictionary indexing. P.B and F.B provided funding and continuous support at all stages. M.M and T.U conducted XRD analysis. M.M wrote the manuscript. All authors reviewed the manuscript and approved it prior to submission.

Declaration of Competing Interest

The authors declare that they have no known competing financial interests or personal relationships that could have appeared to influence the work reported in this paper.

Acknowledgements

The Authors would like to thank Framatome for funding and providing the material for the present study. P.F., R.T. and M.P. acknowledge support from MIDAS EPSRC programme grant ((EP/S01702X/1)). The authors thanks Jean-Paul Vassault and Julien Augereau for sample preparation and follow-up experiments, Mariano Marini for hydriding the samples, and Sylvain Duval for reorientation tests. MDG acknowledges financial support from the National Science Foundation (grant DMR-2203378) as well as use of the computational resources of the Materials Characterization Facility at Carnegie Mellon University supported by grant MCF-677785. The research used UKAEA's Materials Research Facility, which has been funded by and is part of the UK's National Nuclear User Facility and Henry Royce Institute for Advanced Materials. AZTEC® is a registered and unregistered trademark of Oxford Instruments and other third parties.

Supplementary materials

Supplementary material associated with this article can be found, in the online version, at doi:10.1016/j.scriptamat.2023.115768.

References

[1] C.E. Ells, Hydride precipitates in zirconium alloys (A review, J. Nucl. Mater. 28 (2) (1968) 129–151.
[2] D.L. Douglass, The metallurgy of zirconium, At. Energy Rev. (1971) 1–464.
[3] Z. Zhao, M. Blat-Yrieix, J. Morniroli, A. Legris, Characterization of zirconium hydrides and phase field approach to a mesoscopic-scale modeling of their precipitation, Zircon. Nucl. Ind. 15th Int. Symp. (2009).
[4] R.S. Daum, Y.S. Chu, A.T. Motta, Identification and quantification of hydride phases in Zircaloy-4 cladding using synchrotron X-ray diffraction, J. Nucl. Mater. 392 (3) (2009) 453–463.
[5] R. Birch, S. Wang, V. Tong, T.B. Britton, The effect of cooling rate and grain size on hydride formation in Zircaloy-4, J. Nucl. Mater. 513 (2018) 221–225.
[6] N. Badr, et al., Crystal structure of hydride platelets in hot rolled zircaloy-2, characterized with synchrotron X-ray diffraction, S/TEM, and EELS, Zircon. Nucl. Ind. 19th Int. Symp. (2021) 732–761.
[7] F. Long, N.N. Badr, Z. Yao, M.R. Daymond, Towards resolving a long existing phase stability controversy in the Zr-H, Ti-H systems, J. Nucl. Mater. 543 (2021), 152540.
[8] L. Lanzani, M. Ruch, Comments on the stability of zirconium hydride phases in Zircaloy, J. Nucl. Mater. 324 (2–3) (2004) 165–176.
[9] C.E. Coleman, G.A. McRae, A. Buyers, S. Hanlon, Gamma-zirconium hydride on DHC fracture surfaces is a legitimate stable phase, not a metastable phase, J. Nucl. Mater. 548 (2021), 152839.
[10] J.H. Root, W.M. Small, D. Khatamian, O.T. Woo, Kinetics of the δ to γ zirconium hydride transformation in Zr-2.5Nb, Acta Mater 51 (7) (2003) 2041–2053.
[11] S. S. Sidhu, N. S. S. Murthy, F. P. Campos, and D. D. Zauberis, "Neutron and X-Ray diffraction studies of nonstoichiometric metal hydrides," Jan. 1962.
[12] J.E. Bailey, Electron microscope observations on the precipitation of zirconium hydride in zirconium, Acta Metall 11 (4) (1963) 267–280.
[13] S. Mishra, K.S. Sivaramakrihnan, M.K. Asundi, Formation of the gamma phase by a peritectoid reaction in the zirconium-hydrogen system, J. Nucl. Mater. 45 (3) (1972) 235–244.
[14] T. Maimaitiyili, et al., The preparation of Zr-deuteride and phase stability studies of the Zr-D system, J. Nucl. Mater. 485 (2017) 243–252.
[15] S. Banerjee, S.J. Vijayakar, R. Krishnan, Precipitation in zirconium-niobium martensites, J. Nucl. Mater. 62 (2–3) (1976) 229–239.
[16] C. Cann, A. A.-J. of N. Materials, and undefined 1980, "A Metallographic Study of the Terminal Solubility of Hydrogen in Zirconium at Low Hydrogen Concentrations," Elsevier.
[17] K.G. Barraclough, C.J. Beevers, Some observations on the phase transformations in zirconium hydrides, J. Nucl. Mater. 34 (2) (1970) 125–134.
[18] A.I. Kolesnikov, A.M. Balagurov, I.O. Bashkin, A.V. Belushkin, E.G. Ponyatovsky, M. Prager, Neutron scattering studies of ordered gamma -ZrD, J. Phys. Condens. Matter 6 (43) (1994) 8977–8988.
[19] Z. Wang, et al., Observations of temperature stability of γ-zirconium hydride by high-resolution neutron powder diffraction, J. Alloys Compd. 661 (2016) 55–61.
[20] M.P. Cassidy, C.M. Wayman, M.P. Cassidy, C.M. Wayman, The crystallography of hydride formation in zirconium: I. The δ → γ transformation, MTA 11 (1) (1980) 47–56.
[21] J.S. Bradbrook, G.W. Lorimer, N. Ridley, The precipitation of zirconium hydride in zirconium and zircaloy-2, J. Nucl. Mater. 42 (2) (1972) 142–160.
[22] S.M. Hanlon, S.Y. Persaud, F. Long, A. Korinek, M.R. Daymond, A solution to FIB induced artefact hydrides in Zr alloys, J. Nucl. Mater. 515 (2019) 122–134.
[23] F. Long, N.N. Badr, Z. Yao, M.R. Daymond, Characterizing the crystal structure and formation induced plasticity of γ-hydride phase in zirconium, Materialia 8 (2019), 100454.
[24] E. Tulk, M. Kerr, M.R. Daymond, Study on the effects of matrix yield strength on hydride phase stability in Zircaloy-2 and Zr 2.5 wt% Nb, J. Nucl. Mater. 425 (1–3) (2012) 93–104.
[25] M. Maric, et al., Characterisation of hydride precipitation and reorientation in Zircaloy-4 at different metallurgical states, ASTM STP1645 20th Int. Symp. Zircon. Nucl. Ind. (2023).
[26] Z. Ding, E. Pascal, M. De Graef, Indexing of electron back-scatter diffraction patterns using a convolutional neural network, Acta Mater 199 (2020) 370–382.
[27] Y.H. Chen, et al., A dictionary approach to electron backscatter diffraction indexing*, Microsc. Microanal. 21 (3) (2015) 739–752.
[28] S.U. Park, D. Wei, M. De Graef, M. Shah, J. Simmons, A.O. Hero, EBSD image segmentation using a physics-based forward model, in: 2013 IEEE Int. Conf. Image Process. ICIP 2013 - Proc, 2013, pp. 3780–3784.
[29] M. De Graef, A dictionary indexing approach for EBSD, IOP Conf. Ser. Mater. Sci. Eng. 891 (1) (2020), 012009.
[30] M. De Graef et al., "EMsoft-org/EMsoft: Release 4.2 to synchronize with DI tutorial paper," Mar. 2019.
[31] E. Zuzek, J.P. Abriata, A. San-Martin, The H-Zr (hydrogen-zirconium) system, Bull. Alloy Phase Diagrams 11 (4) (1990) 385–395.
[32] K. Moore, Phase studies of the Zr-H system at high hydrogen concentrations, Elsevier, 1968.
[33] D. Northwood, U. K.-I, Hydrides and delayed hydrogen cracking in zirconium and its alloys, Taylor Fr 28 (1) (2013) 92–121.
[34] C.P. Kempter, R.O. Elliott, K.A. Gschneidner, Thermal expansion of delta and epsilon zirconium hydrides, J. Chem. Phys. 33 (3) (1960) 837–840.
[35] E.A. Gulbransen, K.F. Andrew, Crystal structure and thermodynamic studies on the zirconium-hydrogen alloys, J. Electrochem. Soc. 101 (9) (1954) 474.
[36] A.T. Motta, et al., Hydrogen in zirconium alloys: a review, J. Nucl. Mater. (2019).
[37] H. Numakura, M. Koiwa, Hydride precipitation in titanium, Perspect. Hydrog. Met. (1986) 501–509.
[38] A. Steuwer, J. Santisteban, M. Preuss, Evidence of stress-induced hydrogen ordering in zirconium hydrides, Acta Mater 57 (1) (2009) 145–152.
[39] T. Maimaitiyili, J. Blomqvist, A. Steuwer, In situ hydrogen loading on zirconium powder, J. Synchrotron Radiat. 22 (4) (2015) 995–1000.
[40] T. Maimaitiyili, A. Steuwer, C. Bjerkén, J. Blomqvist, The preparation of Zr-deuteride and phase stability studies of the Zr-D system, J. Nucl. Mater. 485 (2017) 243–252.
[41] M. D. Atkinson, R. Thomas, A. Harte, P. Crowther, and J. Quinta da Fonseca, "DefDAP: deformation data analysis in python - v0.93.2," Apr. 2021.
[42] L.T. Hansen, et al., Influence of noise-generating factors on cross-correlation electron backscatter diffraction (EBSD) measurement of geometrically necessary dislocations (GNDs, Microsc. Microanal. 23 (3) (2017) 460–471.
[43] G.J.C.J.C. Carpenter, The dilatational misfit of zirconium hydrides precipitated in zirconium, J. Nucl. Mater. 48 (3) (1973) 264–266.
[44] B.W. Leitch, M.P. Puls, Finite element calculations of the accommodation energy of a misfitting precipitate in an elastic-plastic matrix, MTA 23 (3) (1992) 797–806.
[45] D. Kerr, F. Long, G. Domizzi, M. R. Daymond, and IUCr, "Orientation relationships between α-zirconium and δ-hydride within a hydride blister," *urn:issn:1600-5767*, vol. 50, no. 2, pp. 349–356, Feb. 2017.
[46] S. Wang, et al., Microscopic stress and crystallographic orientation of hydrides precipitated in Zr-1Nb-0.01Cu cladding tube investigated by high-energy X-ray diffraction and EBSD, J. Nucl. Mater. 542 (2020), 152534.
[47] K. Une, K. Nogita, S. Ishimoto, K. Ogata, Crystallography of zirconium hydrides in recrystallized zircaloy-2 fuel cladding by electron backscatter diffraction, J. Nucl. Sci. Technol. 41 (7) (2004) 731–740.
[48] C.. Ellis, Hydride precipitates in zirconium alloys, J. Nucl. Mater. 28 (1968) 129.
[49] Y.J. Jia, I.J. Beyerlein, W.Z. Han, Precipitation characteristics and distributions of subsurface hydrides in zirconium, Acta Mater. 216 (Sep. 2021), 117146.
[50] G.C. Weatherly, The precipitation of γ-hydride plates in zirconium, Acta Metall. 29 (3) (1981) 501–512.